

## Compressive Strength of Axially Loaded Built-up Sigma Cold Formed Sections Columns

Mohamed El Aghoury  
mohamed.elaghoury@fue.edu.eg

Maged Tawfic  
m\_tawfick2003@yahoo.com

Essam Amoush  
essamamoush2008@yahoo.com

Follow this and additional works at: <https://digitalcommons.aaru.edu.jo/fej>



Part of the [Structural Engineering Commons](#)

---

### Recommended Citation

El Aghoury, Mohamed; Tawfic, Maged; and Amoush, Essam () "Compressive Strength of Axially Loaded Built-up Sigma Cold Formed Sections Columns," *Future Engineering Journal*: Vol. 1 : Iss. 3 , Article 2. Available at: <https://digitalcommons.aaru.edu.jo/fej/vol1/iss3/2>

This Original Article/Research is brought to you for free and open access by Arab Journals Platform. It has been accepted for inclusion in Future Engineering Journal by an authorized editor of Arab Journals Platform. For more information, please contact [marah@aarj.edu.jo](mailto:marah@aarj.edu.jo), [dr\\_ahmad@aarj.edu.jo](mailto:dr_ahmad@aarj.edu.jo).

HOSTED BY



Future Engineering Journal

Journal homepage: <http://digitalcommons.aaru.edu.jo/fej/>

# Compressive Strength of Axially Loaded Built-up Sigma Cold Formed Section Columns

## Keywords:

Steel  
Strength, Stability  
Cold Formed Sections  
Built-up sigma columns  
Imperfections

## ABSTRACT

The use of cold formed steel sections in building constructions has lately seen rapid growth due to their light weight and easier erection. Generally, lipped channel sections are used more frequently. Sigma sections while requiring more effort in fabrication, they exhibit high strength to weight ratios compared with the lipped channel sections. This work presents experimental as well as numerical study of the strength of pinned-pinned axially loaded columns utilizing sigma sections. The column section consists of two back to back sigma cold formed sections. The two sections are connected through their webs with connecting fasteners. Eight specimens with variable plate element width to thickness ratio, and having different member slenderness ratios were tested. Residual stresses and geometrical imperfections were recorded. Moreover, the specimens were simulated by a nonlinear finite element model using four node isoparametric shell element that accounts for both geometric and material non-linearities. The measured geometric imperfections and residual stresses were included in the numerical model. The parameters studied include the properties of the cross-section such as the flange, web, and lip dimensions as well as the spacing of the web fasteners. Furthermore, several column heights are considered to study the different modes of failure. Finally, the results are compared with the ultimate strength predicted by the American AISI, the Eurocode-3 and DSM specifications. Results reflect that sectional (local/distortional) buckling governs the failure mode of short columns. Moreover, the AISI, the Eurocode-3 and DSM can reasonably predict the ultimate load capacity of such sections.

© 2019 Faculty of Eng. & Tech., Future University in Egypt. Hosting by Elsevier. All rights reserved.

Peer review under responsibility of Faculty of Eng. & Tech., Future University in Egypt.

## 1. Introduction

Cold-formed steel sections (CFS) have been used extensively by the construction industry in several countries. Built-up cold-formed steel sections are employed when rolled sections do not provide the needed capacity to support the applied loads. They are usually composed of two or more sections connected either back to back to form an "I" section or toe to toe to form a "box" section. It is interesting to note that, the axial compression capacity of built-up members is usually higher than twice that of the constituent elements. Some complexity arises from the interactive buckling characteristic of such members under loads. However, most design codes contain some provisions for the spacing between fasteners and modified slenderness ratios to account for the effect of shear deformation on the overall flexural buckling of built-up (CFS) columns.

Several researchers have reported work in this field. Lau H.H. and Ting T.C.H. (2009), investigated the axial capacity of pin-ended cold-formed steel column using FEM. They used two identical channel sections back to back connected by fasteners at certain spacing along their length. Their results showed that the direct strength method and effective width method were generally conservative for studied columns. Klingshim D. J., et al. (2010), tested fifty-eight sigma shaped specimens under axial compression. To study global, distortional, and local buckling failure modes; specimens having various lengths have been tested. They compared their results with those determined from AISI-2007 design methods, Direct Strength Method and Effective Width Method. Kang T. H. et al., (2013), tested 42 columns to investigate the different buckling modes of built-up cold-formed steel columns. In addition, they determined the effect of the geometrical properties such as plate thickness and width of the member on the axial capacity. Muftah F. et al., (2014), they investigated the importance of bolt or screw arrangement to ensuring that the compound CFS columns can achieve the full sectional strength. In order to prevent premature failure at the end bearing, they suggested that positioning a screw fastener near the end of the column helps the column to

act as a full section. In addition, using a fastener near the end at an edge distance of about 20 mm was found to be very effective in avoiding end bearing failure. Fratamico D. C. et al., (2015), explored the behavior of cold-formed steel compound sections in global flexural buckling using a FEM in static and eigen-buckling analysis. The model included two-dimensional beam elements connected using a special fastener element. Fratamico H. D. et al., (2016) reported an experimental investigation on the buckling behavior of various forms of CFS columns. They tested four types of cross-sections, namely, single, open and two closed built-up. They also included both pinned and fixed end conditions. They found that for the fixed-ended columns the predictions could be conservative, while for pin-ended lipped channel columns the design predictions were in reasonable agreement with the experimental results. Moreover, they concluded that, additional experimental and numerical investigations are needed in the field of built-up CFS structural members using multi-single profiles. Lu Y., et al., (2017), tested a total of 18 compressed single C-section columns and 18 built-up I-section columns under uniaxial compression. They noted that local-distortional interaction occurred for short built-up columns and local-distortional-global interaction for built-up columns of intermediate length. They reported that these interactive modes caused considerable reduction in the ultimate strength of cold-formed built-up I-section columns. They proposed a novel direct strength-based method to quantify such a reduction. Fratamico D. C., et al. (2018), tested back-to-back channels connected through their webs using two self-drilling screw fasteners at specified spacing along the column length. Tests were conducted with two back-to-back studs seated in track with and without sheathing. Results indicated a wide range of deformation behavior, with local global interaction and flexural-torsional modes common in many of the unsheathed specimens. However, all sheathed columns failed in web local buckling and were not markedly influenced by the web interconnection. Distortional buckling was modestly influenced by the end conditions and the web interconnection. The present work aims to study the structural behavior of columns composed of two sigma CFS connected back-to-back by fasteners. The study accounts for the effect of cross-sectional geometric proportions, overall slenderness ratios, and the spacing between fasteners. Both experimental and numerical investigations have been performed. Finally, comparisons of experimental results with those of the finite element model and codes of standard were carried out

### Nomenclature

B	double sigma flange width
D	flange lip depth
H	overall web depth
H1	web remaining parts
H2	web remaining parts
H3	web middle part depth
L	the column length
$P_u$	ultimate load
$P_y$	yielding load
S	the fastener spacing
a	web recesses
b	single sigma flange width
e1	load eccentricities in y-y direction
e2	load eccentricities in x-x direction
$r_i$	the radius of gyration about of the single element about y-y axis
$r_y$	the radius of gyration of the whole section about y-y axis
$\delta$	lateral displacement
$\lambda_c$	overall slenderness ratio of column

## 2. Experimental study

The tested columns are composed of two sigma CFS sections. The sections are placed back to back and connecting by fasteners at the mid height of the column Fig. 1. Each sigma section has an overall web depth,  $H=160$  mm. The depth of the middle part, H3, of the web is kept constant and is equal to 40mm, while the remaining parts, H1& H2, are varied to achieve two ratios of web recess to flange width ratio  $a/B = 0.25$  &  $0.75$ . Two flange widths equal 40 mm and 50 mm are selected. The flange lip depth is equal to 13.3mm. This results in a ratio of flange lip depth to flange width,  $D/B$ , equal to 0.33 and 0.267. The thickness of the section is kept constant at 1mm. Dimensions of the tested specimens are listed in Table (1). The specimens were aligned vertically in the test frame as shown in Fig. 2. The loads were applied at the specimen upper end by a 250 KN jack, while the lower end resists the developed reactions. To ensure equal stresses distribution across the section, two 20 mm thick head plates were bolted to the ends of each specimen. In addition, the ends of each specimen were milled flat to ensure full contact between the specimens and the end bearing plates. The loads were applied to the specimens through hinges placed in a groove made through the thickness of the end plates. These end conditions allow rotation about strong and weak axes, while preventing any lateral translation of the specimen. Moreover, the presence of head plates prevents warping at the ends of the specimens. M6 H.S.B. Grade 8.8 Bolts (fasteners) were used for assembling the specimens and for connecting them to the end plates. Although a theodolite was used to ascertain the vertical alignment of the specimen in the test frame, there were some eccentricities at the ends of all specimens. Detailed measurements of eccentricities at specimen ends (e1& e2) were made and recorded in the laboratory and are listed in Table 2. The axial shortening under load and the

lateral displacement were recorded using the Tokyo-Sokki S-2420 data acquisition system. Three (LVDT) transducers were placed at the mid-height point of the specimen to measure the horizontal displacements of the web mid points and the flange lip juncture points. In addition, one (LVDT), was attached vertically to measure the axial shortening. At the start of the test, one tenth of the estimated ultimate load was applied as initial load. This load was kept constant for about 10 seconds to achieve full contact between the loading jack and the specimen end bearing plate. Tensile coupons were prepared and tested in accordance with ASTM-A370 and results indicating that the steel is mild steel has yield stress and Young's modulus equal to 240MPa, and 200000MPa; respectively. Details of measurements of geometric imperfections and residual stresses are reported in El Aghoury M. A., et al., (2014).

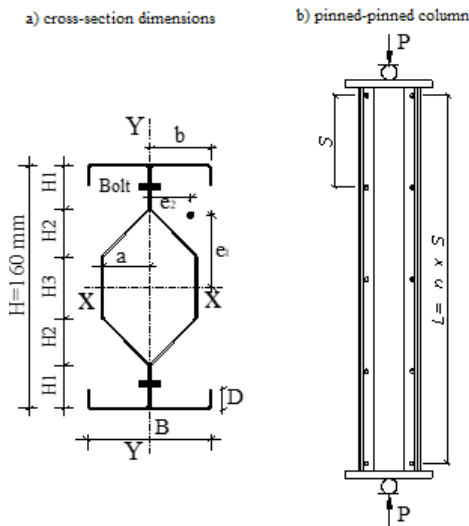


Fig. 1- column geometry and cross-section dimensions

Table 1 - Test specimen dimensions.

Specimen	Section Dimensions (mm)							L (mm)
	H	H1	H2	H3	B	D	a	
S40-25-50	160	50	10	40	40	13.3	10	895
S40-25-100	160	50	10	40	40	13.3	10	1788
S40-75-50	160	30	30	40	40	13.3	30	1125
S40-75-100	160	30	30	40	40	13.3	30	2250
S50-25-50	160	47.5	12.5	40	50	13.3	12.5	1140
S50-25-100	160	47.5	12.5	40	50	13.3	12.5	2282
S50-75-50	160	30	30	40	50	13.3	30	1142
S50-75-100	160	30	30	40	50	13.3	30	2500

Note, L is the height of the specimens

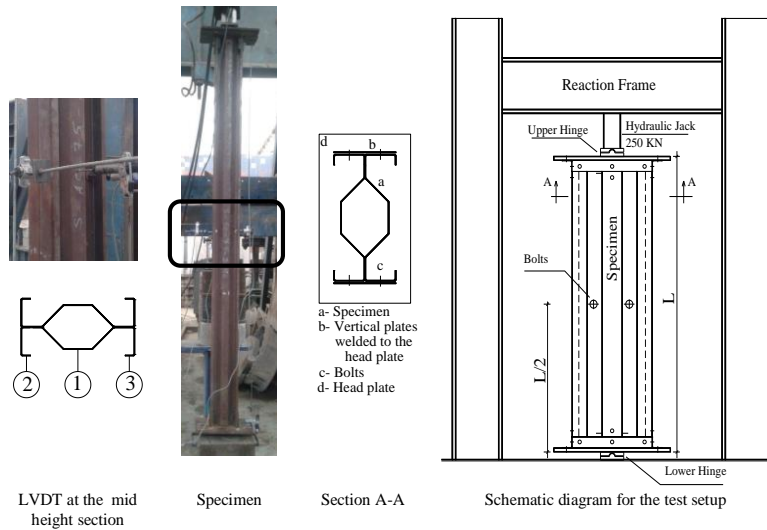


Fig. 2 - experimental setup

### 3. Numerical finite element model

The tested specimens were simulated by a three-dimensional finite element model. The modeling was conducted using the general-purpose finite element software package ANSYS 12.0.1. Both geometric and material non-linearities were accounted for in the elasto-plastic finite element model. The columns were modeled using 4-node shell element, SHELL181. This element has six degrees of freedom at each node, 3 translations and 3 rotations, to allow for the explicit simulation of various buckling modes. Besides, this element is suitable for modeling thin to moderately-thick shell structures with both elastic and elasto-plastic material behavior. To provide adequate accuracy, the elements comprising the mesh have aspect ratios close to one. In addition, fasteners that connect column webs are modeled using the contact element CONTA178. This element is capable of supporting compression in the normal direction of the contact area as well as friction in the tangential direction. ANSYS classical metal plasticity model was used to account for the effect of material non-linearity. This model implements the von-Mises yield surface to define isotropic yielding and associated plastic flow theory. A perfect plasticity model based on a simplified bilinear stress-strain curve without strain hardening was assumed. The elastic modulus of elasticity and yield stress of the steel material were considered as 200000 MPa and 240 MPa; respectively. The shear modulus was taken equal to 81000 MPa. The end conditions for column centre line are treated as pinned. However, warping of the column end cross section is restrained due to presence of thick end plates. The loaded end was prevented from rotation about z-axis and translations in X and Y directions. On the other hand, the unloaded end was prevented from translation in the three directions X, Y and Z and from rotations about the z-axis. The loads were applied at loaded end of the column with eccentricities about X and Y axes similar to those measured in the tests. Figure 3 shows the finite element model, loads, and boundary conditions. The load was incrementally increased through successive load steps. Newton-Raphson iterations were used in solving the nonlinear system of equations. As was noted in El Aghoury M. A., et. al., [10], the ultimate loads are sensitive to the overall geometric imperfection modes rather than local imperfection ones, therefore, the column was modeled with a half-sine wave bending about the minor axis "Y". The imperfection value considered is  $L/1000$ , where L is the column length. In addition, the residual stress pattern was assumed as given in El Aghoury M. A. et. al., (2014). The numerical model results are plotted in Fig. 4 along with the test results for specimens S50-25-50 and S50-25-100; where the applied load, P, is plotted against the lateral displacement,  $\delta$ , of the mid-height point of the web as well as the axial shortening. Numerical and experimental results of the tested specimens are listed in Table 2. Generally, there is good agreement between the experimental and numerical results. In addition, the failure shapes predicted by the finite element model are comparable to the test results, and the distortional buckling half wave lengths are very close to that measured in the lab as depicted in Fig. 5



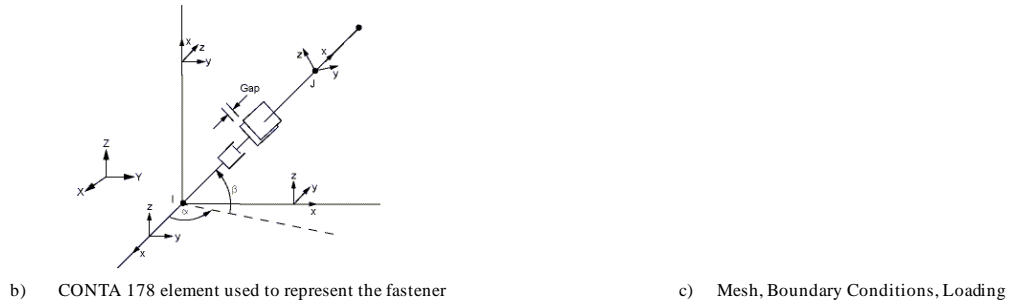


Fig. 3 - finite element model

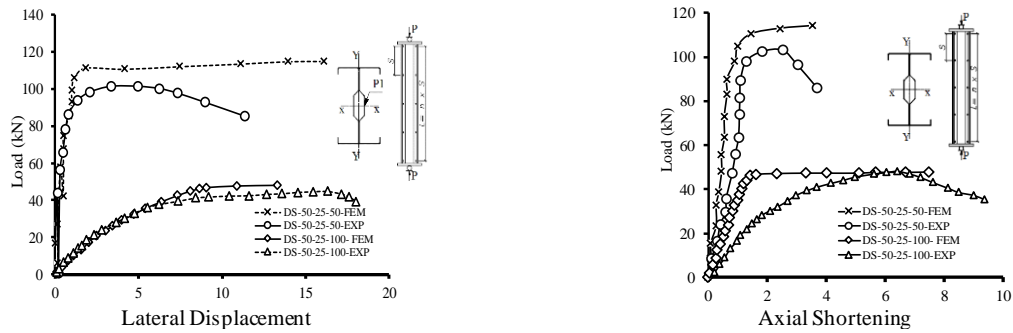


Fig. 4 - load versus lateral displacements and axial shortening for specimens 50-25-50 & 50-25-100

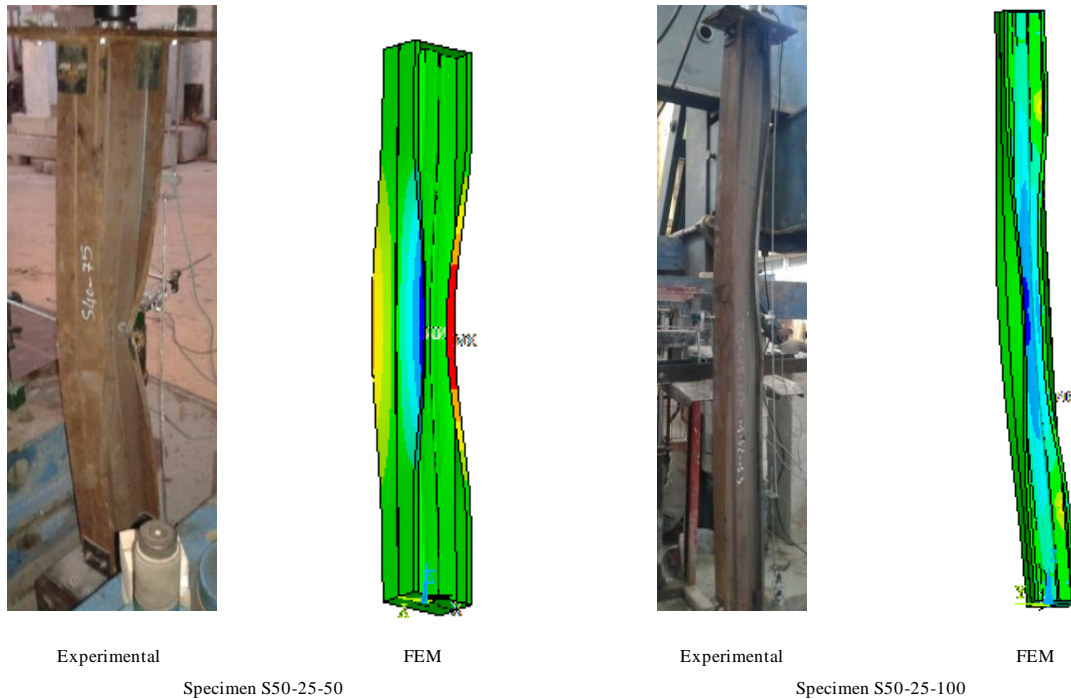


Fig. 5 - failure modes of specimens S50-25-50 & S50-25-100

Table 2 - Test results

Specimen	$\lambda_c$	a/B	D/B	$e_1$ (mm)	$e_2$ (mm)	$P_u$ (kN)					
						Experimental		FEM			
						$P_u$	$P_u/P_y$	$P_{u1}$	$P_{u1}/P_y$	$P_{u2}$	$P_{u2}/P_y$
S40-25-50	0.68	0.25	0.33	12	25	68	0.52	73	0.56	118	0.91

S40-25-100	1.37	0.25	0.33	----	----	57	0.43	61.9	0.47	61.8	0.47
S40-75-50	0.88	0.75	0.33	----	----	102	0.74	115	0.83	115	0.84
S40-75-100	1.77	0.75	0.33	20	----	57	0.41	57	0.41	84	0.61
S50-25-50	0.7	0.25	0.26	----	----	102	0.72	112.6	0.8	112	0.8
S50-25-100	1.4	0.25	0.26	8	25	48	0.34	48	0.34	63.5	0.45
S50-75-50	0.7	0.75	0.26	18	----	93	0.63	93.5	0.63	126	0.86
S50-75-100	1.55	0.75	0.26	----	----	60	0.4	64.2	0.43	64.2	0.43

Note,  $P_{u1}$ : Ultimate loads considering eccentricities  $e1$  &  $e2$

$P_{u2}$ : Ultimate loads neglecting eccentricities  $e1$  &  $e2$

In cold-formed sections there are three basic failure modes. These are local buckling that involves rotation at internal folds, distortional buckling that involves both rotation and translation of internal fold lines and overall buckling that involves “rigid-body” deformation of the cross-section without distortion. On this basis the deformed shapes observed can be regarded as the result of distortional buckling for short columns. However, in long columns the mode of failure is overall bending in addition to the distortional buckling of the flanges.

#### 4. Parametric numerical study

The numerical finite element model is used to make an extended parametric study. In this study, the web full depth of the column cross-section and the web thickness are kept constant at 160 mm and 1mm; respectively. However, the middle web dimensions, H1, H2 and H3, and the flange width, B, are varied to introduce different proportions of the cross sections. The lip depths were selected so that they possess enough inertia to fully stiffen the flanges. Both lipped as well as unlipped sections are studied. The section dimensions are listed in Table 3. To add on, different member lengths, L, and fastener spacing, S, are included in the study. Note that, the label “S20-25-80-U” is defined as follows: the first letter “S” represents the cross section profile (sigma), while, the second two digits “20” indicate the flange width-to-thickness ratio, b/t, the following two digits “25” give the ratio of the inward recess of the web (middle part) to the flange width a/b. The last two digits “80” indicate the inner web width-to-thickness ratio, H3/t, and the last letter “U” indicates that the section is unlipped.

**Table 3 - dimensions of specimens investigated numerical studied sections**

Specimen	Section Dimensions (mm)					b/t	H3/t	a/b
	H1	H2	H3	b	a			
S20-25-20-U S20-25-20-L	65	5	20	20	5	20	20	0.25
S20-25-80-U S20-25-80-L	35	5	80	20	5	20	80	0.25
S50-25-20-U S50-25-20-L	57.5	12.5	20	50	12.5	50	20	0.25
S50-25-80-U S50-25-80-L	27.5	12.5	80	50	12.5	50	80	0.25
S20-75-80-L	22.5	17.5	80	20	17.5	20	80	0.75
S50-75-20-L	32.5	37.5	20	50	37.5	50	20	0.75

Note,  $t = 1\text{ mm}$

The effect of fasteners spacing on the ultimate loads of the combined sections,  $P_u$ , was first determined. The normalized ratio,  $P_u/P_y$ , is plotted in Figs. 6 & 7 as a function connecting fastener spacing.

Close examination of the results reveals that in sections with large interior web width to thickness ratio,  $H3/t = 80$ , the ultimate loads decrease as the spacing between the connecting fasteners increases. For instance, the ratio  $P_u/P_y$  of columns S-20-25-80-L ( $L/r_y = 100$ ) decreased by 30% when the fastener spacing, S, increased from L/4 to L/2. Similarly, the maximum capacity,  $P_u/P_y$ , of column sections S-50-25-80-L ( $L/r_y = 100$ ) are 0.44 and 0.37 for connecting fastener spacing equal to L/4 and L/2; respectively. On the other hand, the spacing of the connecting fastener does not greatly influence the ultimate loads of columns with sections having small web width to thickness ratios,  $H3/t=20$ . Columns with sections S-20-25-20-L exhibited ratios  $P_u/P_y$  of 0.48 and 0.45 for fastener spacing L/4 and L/2 respectively. Also, El Aghoury M. A., et. al., (2016) showed that the ultimate loads of sections with interior web width to thickness ratios,  $H3/t$ , equal to 40 decreased slightly with the increase of the connecting fastener spacing.

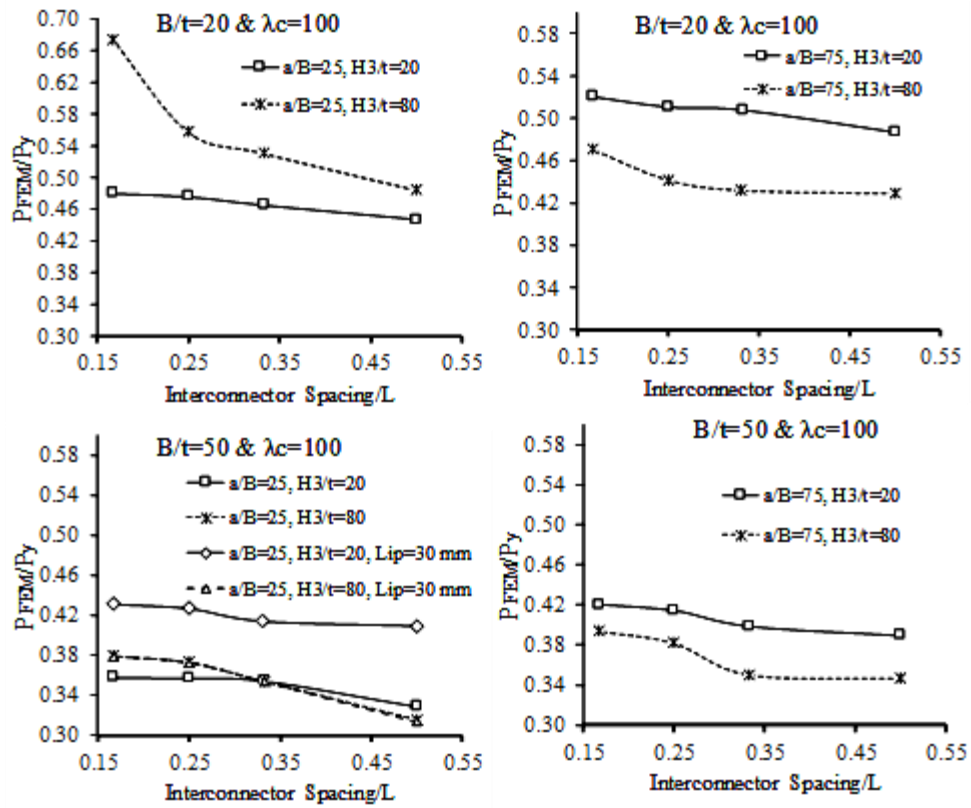
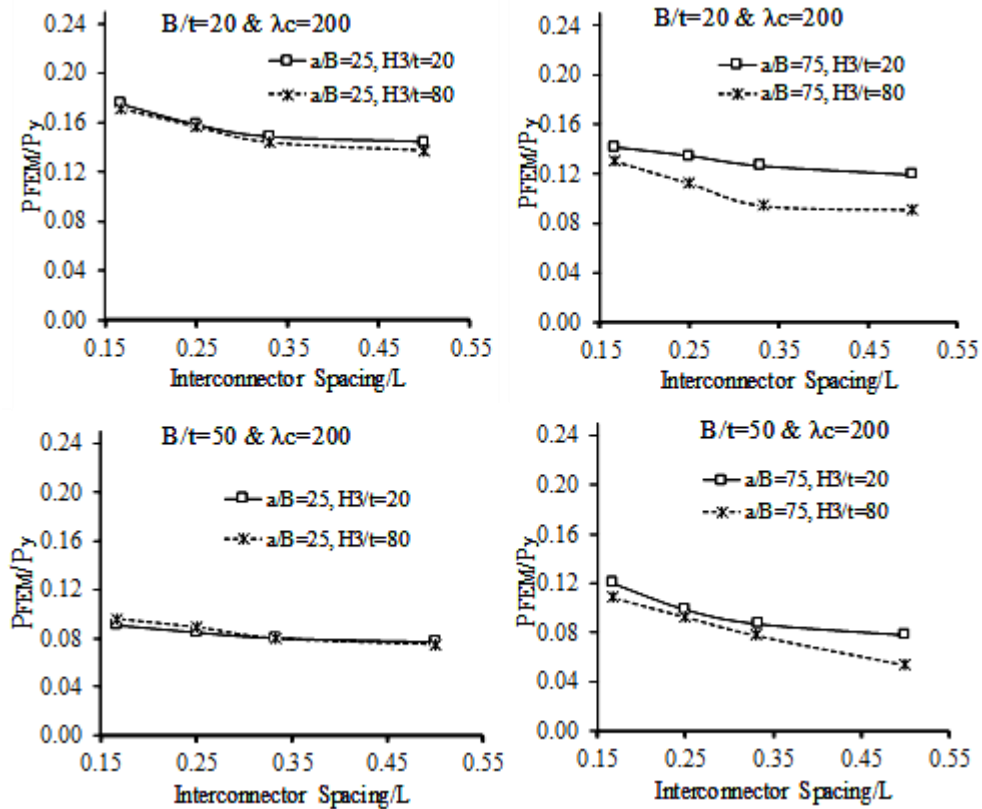
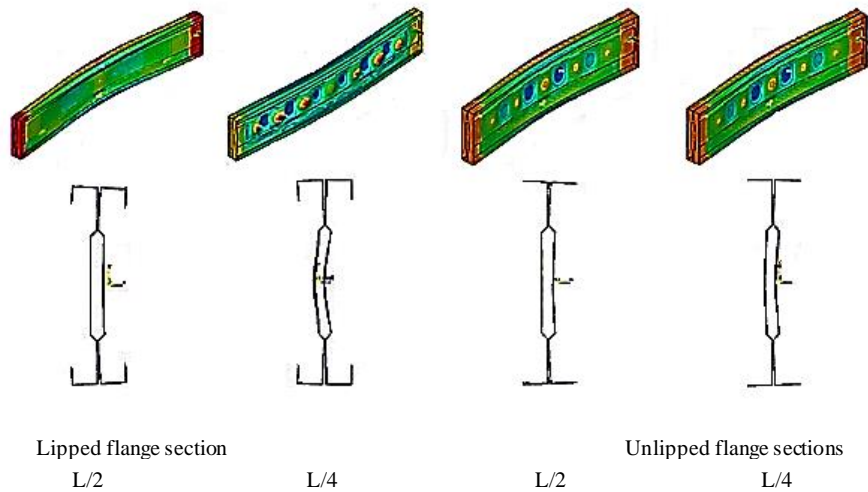


Fig. 6 - ( $P_{FEM}/P_y$ ) versus interconnector spacing for columns having ( $\lambda_c=100$ )



**Fig. 7 - ( $P_{FEM}/P_y$ ) versus different interconnector spacing for columns ( $\lambda_c=200$ )**

The failure modes are characterized by interactive overall sectional (local/distortional) buckling, for columns with moderate overall member slenderness ratios,  $\lambda_c=100$ . However, sections with large interior web width to thickness ratios,  $H3/t = 80$ , experienced clear local buckling waves in the web in addition to the overall buckling mode. These waves are clearly visible for columns with connecting fastener spacing equal  $L/4$ . Moreover, for sections having higher values of web recess depth to thickness ratio the sectional buckling mode changes from distortional buckling to local buckling if the spacing of connecting fasteners is decreased. Additionally, the rotational stiffness of the flange web juncture is enhanced when the spacing between webs connecting fasteners decreases as shown in Figs 8, 9 and 10. Further, in the un-lipped flange sections, additional distortional buckling waves are formed in the flanges. In sections with low interior web width to thickness ratios,  $H3/t = 20$ , failure modes are mainly interactive distortional buckling in the flanges accompanied by overall member buckling. However, in sections with unlipped flanges having,  $b/t = 50$ , some local buckling waves are visible in the flanges. Additionally, in long columns having,  $L/r_y = 200$ , the observed failure modes are mainly overall buckling. Failure modes are depicted in Figs. 8 & 9 for columns with sections having  $H3/t = 80$ , while Fig. 11 shows the failure modes of columns having  $H3/t = 20$ .



**Fig. 8 - Failure modes of sections with  $b/t = 20$ ,  $H3/t = 80$ ,  $L/r_y = 100$**

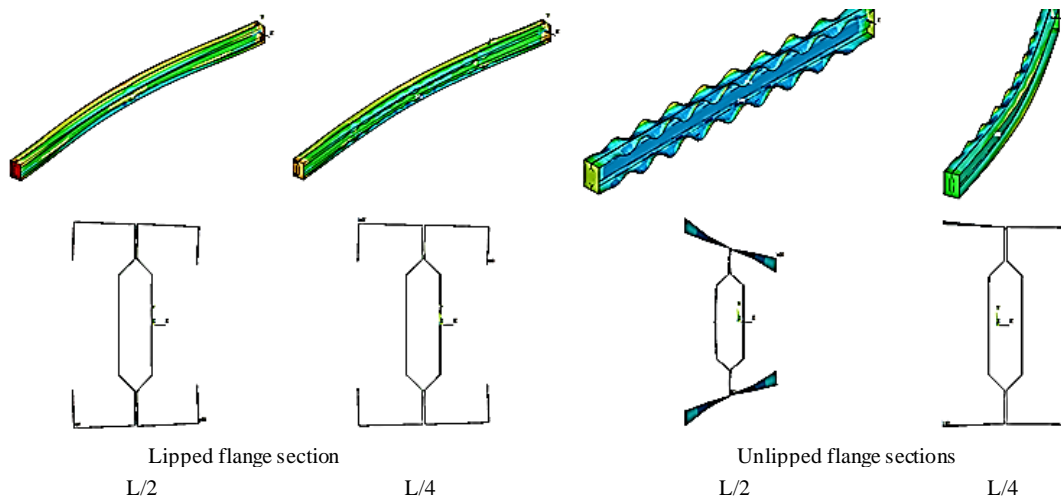
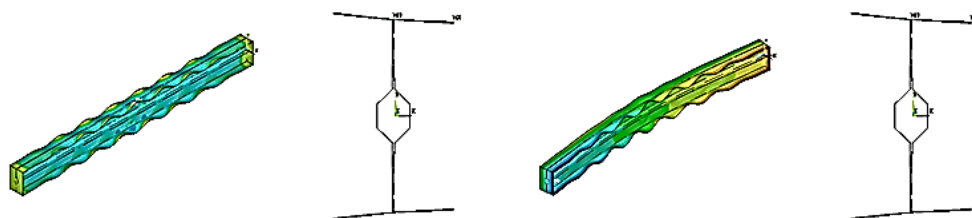


**Fig. 9 - Failure modes of columns sections having  $b/t = 50$ ,  $H3/t = 80$ ,  $L/r_y = 100$**



L/2

L/4

Fig. 10: Failure modes of columns sections having b/t = 50, H3/t = 20, L/ry = 100

5. Comparison with standard codes

In this section, the ultimate capacities of the compound sigma section columns are determined using the design rules provided in Eurocode-3 (2001), AISI-2012, and the direct strength method, DSM, (2002). According to Eurocode-3 and AISI-2012, determination of the design loads is based on the effective width concept, where the ultimate capacities are calculated as the product of the reduced sectional area and the maximum stress,  $F_n$ . The latter will be the lower of the yield stress and the flexural buckling stress which is determined using the full section properties. In the DSM, the axial strength will be the lowest of the local, distortional, and the overall buckling strengths. This method requires the calculation of the elastic critical local and distortional buckling stresses. The values of these stresses are determined using CUFEM computer program. Results of this comparison are listed in Table 4, in which the FEM ultimate loads represent the results corresponding to fastener spacing equal to L/4. Moreover, in AISI-2012, the loads are calculated using the modified slenderness ratio given in Equation (1).

$$\left(\frac{KL}{r}\right)_m = \sqrt{\left(\frac{KL}{r}\right)_{y_0}^2 + \left(\frac{s}{r_i}\right)^2} \tag{1}$$

where  $(KL/r)_{y_0}$  is the overall slenderness ratio of the member about y-axis,

s is the fasteners spacing, and

$r_i$  is the radius of gyration of the single element about y-axis

It is interesting to point out that the elastic buckling behavior of the built-up sigma sections is the basis for assessing the capabilities of DSM Schafer (2002) to predict the ultimate loads of such sections. In the model, the nodal lines that correspond to the connecting fasteners location are constrained. This modeling assumed that the webs of the two sections are connected along the whole length of the columns. Results are depicted in Figs. 11 and 12 for wide flange sections (B = 50) with ratios a/B = 0.25 and 0.75; respectively. It is noted that, increasing the ratio a/B increases both the critical local and distortional buckling loads. Moreover, for the sake of comparison, the results corresponding to single sections are added to the figure.

The comparison reveals that the results of the three design codes are comparable and, in some cases slightly higher than the ultimate loads predicted by the Finite Element Model, especially for sections with large interior web width to thickness ratios, H3/t = 80. This is intuitively explained as a result of the codes limits for the ratio of interconnector spacing to radius of gyration of an individual shape does not exceed one-half the governing slenderness ratio of the built-up member as indicated in Equation (2) (AISI-2012, provision, D1.2). Thus, the capacities are calculated assuming full contact between the two sections.

Table 4 - Comparison with design codes

Specimen	KL/ry	Pu/Py				$\frac{P_{FEM}}{P_{EURO}}$	$\frac{P_{FEM}}{P_{AISI}}$	$\frac{P_{FEM}}{P_{DSM}}$
		FEM	Eurocode-3	AISI-2012	DSM			
S20-25-20-L	100	0.47	0.48	0.5	0.55	0.98	0.94	0.85
S20-25-80-L	100	0.69	0.49	0.51	0.57	1.4	1.35	1.21
S50-25-20-L	100	0.42	0.48	0.46	0.4	0.87	0.91	1.05
S50-25-80-L	100	0.42	0.46	0.44	0.55	0.91	0.95	0.76
S20-25-20-U	100	0.51	0.49	0.48	0.54	1.02	1.06	0.94
S20-25-80-U	100	0.64	0.48	0.48	0.62	1.33	1.33	1.03
S50-25-20-U	100	0.31	0.44	0.41	0.39	0.7	0.75	0.79
S50-25-80-U	100	0.51	0.44	0.37	0.4	1.11	1.37	1.27
S20-75-80-L	100	0.59	0.48	0.51	0.55	1.22	1.15	1.07
S50-75-20-L	100	0.42	0.47	0.47	0.58	0.89	0.89	0.72
S20-25-20-L	200	0.14	0.17	0.155	0.18	0.82	0.93	0.77
S20-25-80-L	200	0.15	0.16	0.156	0.19	0.94	0.96	0.78
S50-25-20-L	200	0.12	0.16	0.19	0.18	0.75	0.63	0.67
S50-25-80-L	200	0.22	0.16	0.18	0.185	1.37	1.22	1.18
S20-25-20-U	200	0.15	0.16	0.125	0.19	0.93	1.20	0.78
S20-25-80-U	200	0.15	0.17	0.124	0.16	0.88	1.21	0.94
S50-25-20-U	200	0.09	0.157	0.146	0.18	0.57	0.62	0.5
S50-25-80-U	200	0.27	0.157	0.138	0.182	1.72	1.95	1.5
S20-75-80-L	200	0.12	0.16	0.167	0.17	0.71	0.78	0.7

S50-75-20-L	200	0.12	0.16	0.14	0.189	0.85	0.13	0.63
Mean, $P_m$						1.00	1.02	0.91

However, the spacing  $S = L/4$  in the studied cases is slightly larger than this limit. The ultimate capacities,  $P_u/P_y$ , of specimens S50-25-20-L and S50-25-50-L for different bolt spacing,  $s$ , are given in Table 5. It is obvious that the ultimate strength increases with decreasing the bolt spacing, especially for sections with large web width to thickness ratios,  $H3/t$ , and the mode of failure changes as depicted in Fig. 13.

$$S \leq \frac{r_i L}{2r_y} \tag{2}$$

where  $L$  = overall member length

$r_i$  = radius of gyration of the single section about  $y$ -axis

$r_y$  = radius of gyration of the whole section about  $y$ -axis

**Table 5 -  $P_u/P_y$  for different bolt spacing,  $s$ .**

Specimen	Bolt spacing, $s$		
	$L/2$	$L/4$	$L/6$
S50-25-20-L	0.4	0.42	0.42
S50-25-80-L	0.37	0.42	0.63

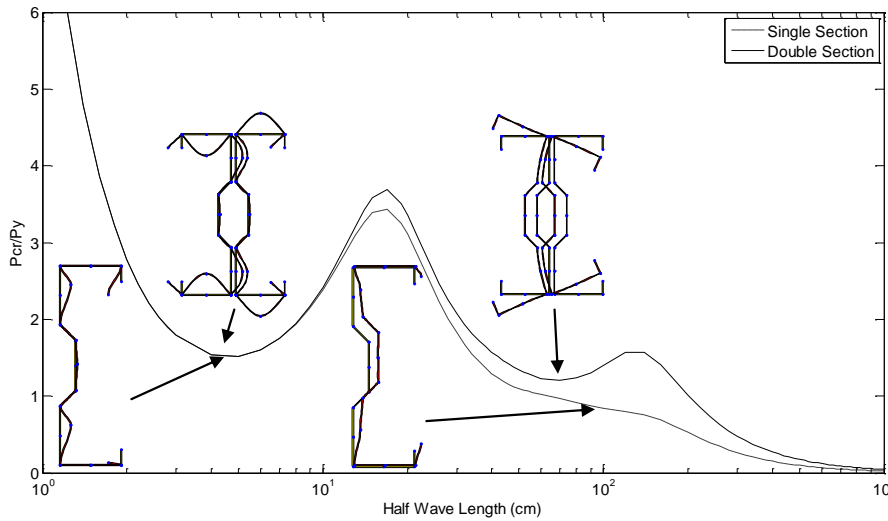


**Fig. 11 - elastic buckling loads of column specimen S50-25**

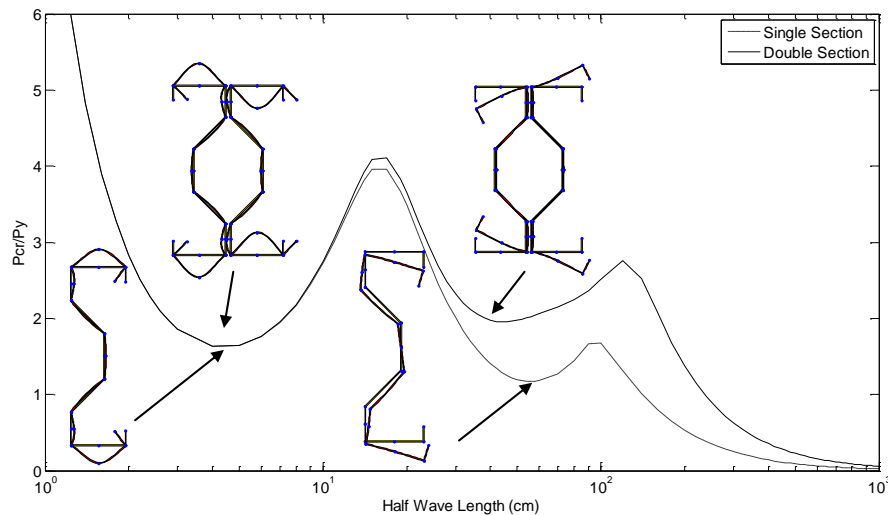


**Fig. 12: Elastic buckling loads of column specimen S50-75**

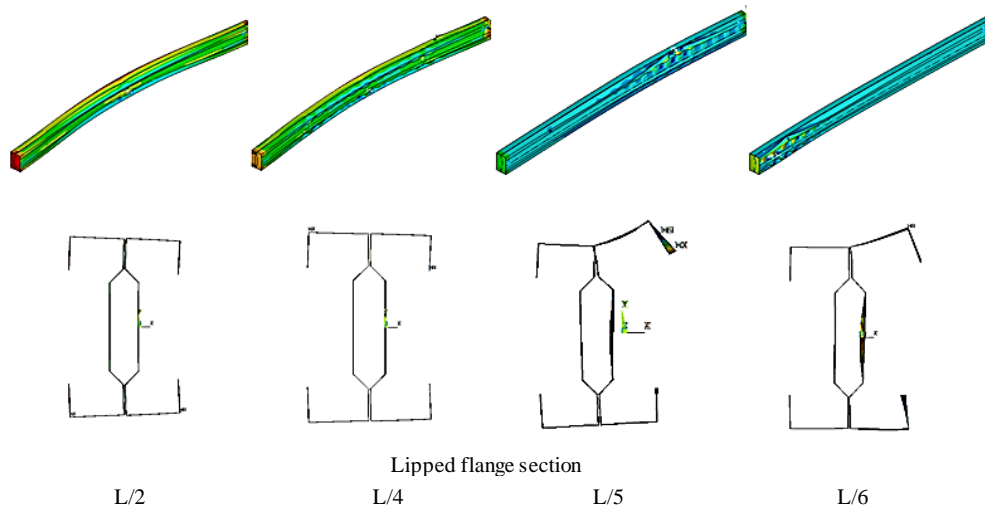


Fig. 13 - failure modes of columns sections having  $b/t = 50$ ,  $H3/t = 80$ , for different fastener spacing, ( $L/r_y = 100$ )

## 6. Conclusions

In this paper, the axial compressive strength of columns consist of back to back cold formed sigma sections is investigated experimentally and numerically. In the tests, it is found that the failure modes of short columns are governed by distortional buckling of the flanges. However, for columns having intermediate height, the failure mode is the interactive distortional overall buckling. The failure modes predicted by the finite element model are comparable with the test results. Further, although the ultimate strength of sections with large interior web width to thickness ratios goes down significantly as the spacing between the connecting fastener increases, strength of sections having small web width to thickness ratios is only slightly affected by fastener spacing. This is also observed experimentally. In-addition, failure modes of intermediate height columns are interactive overall-sectional (local/distortional) buckling mode, while in long columns it is mainly overall buckling. Moreover, for sections having higher values of web recess depth to thickness ratio the sectional buckling mode changes from distortional buckling to local buckling if the spacing of connecting fasteners is decreased. Additionally, the rotational stiffness of the flange web juncture is enhanced when the spacing between webs connecting fasteners decreases. This causes higher critical distortional buckling loads compared with that of the single sigma sections. Moreover, comparison with the design codes reveals that, the predicted ultimate loads of the three codes, Eurocode-3, AISI, and DSM are comparable. In addition, the limit of the spacing between fasteners that is defined in AISI is necessary to achieve the ultimate capacity of the sections.

## REFERENCES

- Lau H. H. and Ting T. C. H., (2009). An investigation of the compressive strength of cold-formed steel built-up I-sections. *Proceedings of Sixth International Conference on Advances in Steel Structures*, Hong Kong, China.
- Klingshim D. J., Sumner E. A., and Rahman N. A., (2010). Experimental investigation of optimized cold-formed steel compression member. *Twentieth International conference on cold formed steel structures*, St. Louse, Missouri, U.S.A., November.
- Kang T. H., Biggs K. A., and Ramseyer C., (2013). Buckling modes of cold-formed steel columns. *IACSIT International Journal of Engineering and Technology*, 5(4).
- Muftah F., Sani I.M. S., Muda M. F. and Shahrin M. (2014). Assessment of connection arrangement of built-up cold-formed steel section under axial compression. *Advanced Materials Research*, 1043, pp 252-257.
- Fratamico D. C., Torabian S., Schafer B. W. (2015 ). Composite action in global buckling of built-up columns using semi-analytical fastener element. *Proceedings of the Annual Stability Conference Structural Stability Research Council Nashville, Tennessee, March*.
- Craveiro H. D., Rodrigues J. P. C., Laim L. (2016). Buckling resistance of axially loaded cold-formed steel columns. *Thin-Walled Structures*, 106, pp 358–375.
- Lu Y., Zhou T., Li W., Wu H. (2017). Experimental investigation and a novel direct strength method for cold-formed built-up I-section columns. *Thin-Walled Structures*, 112, pp 125–139.
- Fratamico D. C., Torabian S., Zhao X, Rasmussen K. J.R., Schafer B. W. (2018). Experiments on the global buckling and collapse of built-up cold-formed steel columns" *Journal of Constructional Steel Research* 144, pp 65–80.
- Fratamico D. C., Torabian S., Zhao X, Rasmussen K. J.R., Schafer B. W. (2018). Experimental study on the composite action in sheathed and bare built-up cold-formed steel columns. *Thin-Walled Structures* 127, pp 290–305.
- El Aghoury M. A., Hanna M. T. and Amoush E. A. (2104). Effect of initial imperfections on axial strength of cold formed steel single lipped sigma section. *Eurosteel 2014, Naples, Italy, September*.
- ANSYS, Version 12.0.1, Swanson Analysis Systems, Houston, PA. Desalvo, G. J., and Gorman, R. W.,
- El Aghoury M. A., Hanna M. T. and Amoush E. A. (2106). Axial stability of columns composed of combined sigma CFS. *Proceedings of the Annual Stability Conference Structural Stability Research Council Orlando, Florida, April*.
- Eurocode 3, (2001). Design of steel structures. *prEN1993-1-1*, final draft, September.
- American Iron and Steel Institute, AISI, (2012). Cold-formed steel design manual.

Schafer B. W.,(2002). Design manual for the direct strength method of cold-formed steel design. *Final Report to the American Iron and Steel Institute, Washington, DC.*

CUFSM V3.12, . Elastic Buckling Analysis of Thin-Walled Members by Finite Strip Analysis. <http://www.ce.jhu.edu/bschafer/cufsm>.